

Mechanical plasticity of cells

Navid Bonakdar^{1,2*}†, Richard Gerum^{1†}, Michael Kuhn¹, Marina Spörrer¹, Anna Lippert¹, Werner Schneider¹, Katerina E. Aifantis³ and Ben Fabry¹

Under mechanical loading, most living cells show a viscoelastic deformation that follows a power law in time¹. After removal of the mechanical load, the cell shape recovers only incompletely to its original undeformed configuration. Here, we show that incomplete shape recovery is due to an additive plastic deformation that displays the same power-law dynamics as the fully reversible viscoelastic deformation response. Moreover, the plastic deformation is a constant fraction of the total cell deformation and originates from bond ruptures within the cytoskeleton. A simple extension of the prevailing viscoelastic power-law response theory with a plastic element correctly predicts the cell behaviour under cyclic loading. Our findings show that plastic energy dissipation during cell deformation is tightly linked to elastic cytoskeletal stresses, which suggests the existence of an adaptive mechanism that protects the cell against mechanical damage.

The rheological properties of the cell and its cytoskeleton, in particular the complex elastic modulus, define the forces that are necessary to deform the cell, for example during migration through small pores and constrictions². These properties are governed by a small set of fundamental, universal laws: cell rheology is timescale free¹; cells are predominantly elastic over timescales up to minutes, with a stiffness that scales linearly with the contractile prestress of the cytoskeleton³; and under mechanical force, cells both stiffen and fluidize⁴. These fundamental laws are interrelated through the principles of soft glassy physics^{5,6}. The theory of soft glassy rheology predicts that the cell deformation in response to a sudden increase in the mechanical load—the so-called creep response—follows a power law in time^{7,8}. How cells respond after the mechanical load has been removed, however, has thus far not been explored systematically. Does the cell eventually return to its undeformed state like an elastic solid⁹, or does it fail to completely recover like a fluid^{10,11} or a material that has plastically and irreversibly yielded under force¹²? The answer to this question is of fundamental importance, for example, for the transit of neutrophils through capillaries, the injury of lung epithelial cells due to excessive stretch during ventilation, or the response of muscle cells to repeated mechanical loading^{13–15}. Current understanding suggests that cells promptly fluidize and soften after they are transiently stretched¹⁶. Our experimental data on living cells show an incomplete shape recovery after force application, but with a dynamics that exactly matches the dynamics during force application. We also show that the apparent stretched-induced fluidization and softening of cells is attributable to plastic yielding events within the cytoskeleton that reset the zero-stress length of load-bearing elements. A subsequent cell stretch beyond this new zero-stress length therefore proceeds with the original cell stiffness and fluidity.

Incomplete cell shape recovery after force application

The deformation of cells in response to a sudden increase in force has been shown to follow a weak power law in time, regardless of cell type, measurement probe, or measurement method^{1,17,18}. From this, a power-law recovery of cell deformation would be expected when the force is removed. Indeed, cell shape recovery after force application using an optical stretcher has recently been shown to follow a timescale-free (power-law) recovery, but the parameters of this recovery are not linked to the cell mechanical behaviour during force application and predict unphysiologically large negative deformations after longer recovery times¹⁹. Therefore, a sufficiently long waiting time after completion of force application is required to distinguish between different relaxation processes and to answer the question if cell shape relaxation is complete or permanently incomplete.

After a brief force application with magnetic microbeads coupled via integrin-type adhesion receptors to the cytoskeleton, we find that the cell does not completely recover to its original shape even after a waiting time of more than 50 times the duration of force application (Fig. 1a). The deformation $d(t)$ of the cell in response to a step increase in force, ΔF , closely follows a power law over time, $d(t) = c\Delta F(t/t_0)^\beta$, in agreement with previous findings^{17,18,20}. The power-law exponent β reflects the dynamics of the force-bearing structures of the cell that are connected to the bead¹. A power-law exponent of $\beta = 0$ is indicative of a purely elastic solid, and $\beta = 1$ is indicative of a purely viscous fluid. In cells, β usually falls in the range between 0.1 and 0.5, indicating viscoelastic behaviour, whereby higher values have been linked to a higher turnover rate of cytoskeletal structures¹. The parameters of this power law (the power-law exponent β , and the cell compliance c after a force duration of $t_0 = 1$ s), however, overestimate the cell shape recovery after force removal (Fig. 2a) that would be predicted by the Boltzmann superposition principle. This principle is illustrated in Fig. 2a and states that the deformation response $d(t)$ of the cell after the force has returned to zero at time $t = t_1$ can be regarded as the sum of two terms, d_+ and d_- . Here, $d_+(t) = c\Delta F(t/t_0)^\beta$ is the ongoing creep deformation that would arise if the force continues beyond t_1 , and $d_-(t) = -c\Delta F((t - t_1)/t_0)^\beta$ is the deformation that would arise if a negative force of the same magnitude is applied at $t = t_1$ (ref. 21). Moreover, as first noted in ref. 22, the shape recovery after the force has returned to zero is considerably slower than predicted by the response curve during force application. The failure to predict the time course and magnitude of the cell shape recovery from Boltzmann superposition (Fig. 2a) implies that part of the deformation during force application may have been nonlinear or non-reversible, possibly due to the presence of an additional plastic or viscous component.

¹Department of Physics, University of Erlangen-Nuremberg, 91054 Erlangen, Germany. ²Max-Planck Institute for the Science of Light, 91058 Erlangen, Germany. ³Department of Civil Engineering and Engineering Mechanics, University of Arizona, Tucson, Arizona 85721, USA. †These authors contributed equally to this work. *e-mail: navid.bonakdar@mpl.mpg.de

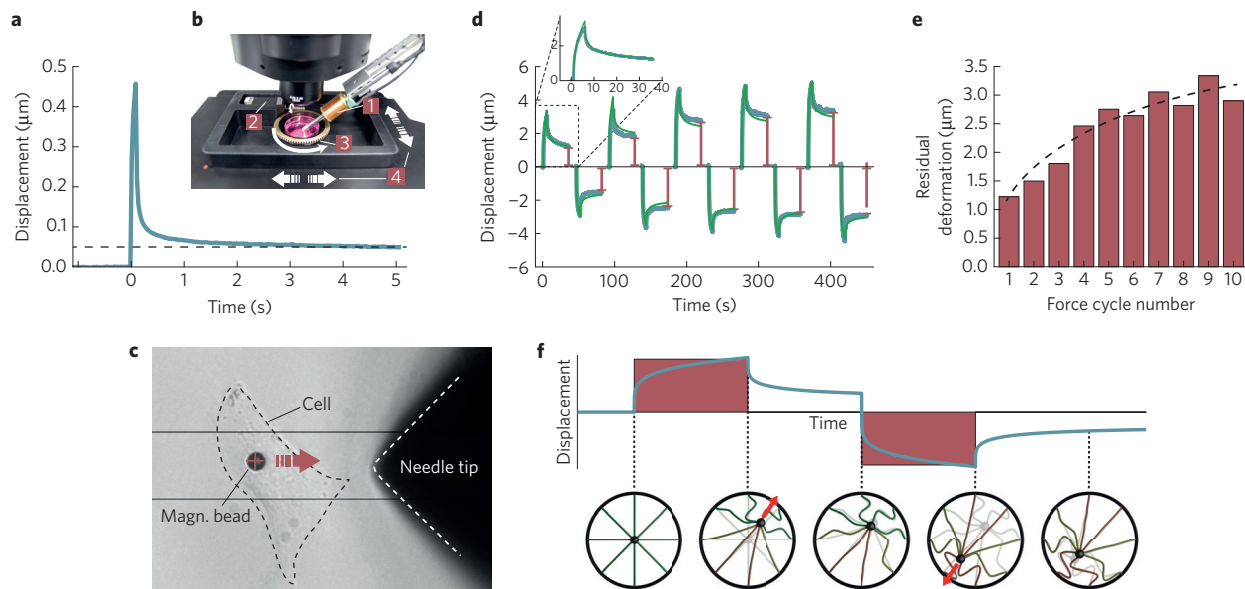


Figure 1 | Cell shape recovery after force application is incomplete. **a**, Incomplete relaxation of cell deformations after force application of 10 nN for 0.1 s duration. Relaxation time is 5 s. **b**, Experimental set-up for multidirectional magnetic force application. A culture dish (3) is rotated with a stepper motor (2). Bead position relative to the fixed needle tip of the magnetic tweezer (1) is corrected after rotation with the motorized x-y stage (4) of the microscope (see Supplementary Movie 1). **c**, Bright-field image of a cell with attached bead and magnetic tweezer tip. **d**, Bead displacements (light blue lines) in response to 10 nN force steps (duration 3 s) in alternating directions. Bead positions at the beginning of each force cycle are set to zero. Bead displacements show an increasing magnitude of incomplete recovery at the end of each force cycle (red bars). Displacements are fitted with equations (1) and (2) for positive and negative forces separately (green). **e**, Amplitude of incomplete recovery versus force cycle number follows a weak power law (black line). **f**, Simplified model describing the evolution of plastic deformations and slack in cytoskeletal structures in response to alternating forces. Tensed fibres are permanently stretched, while compressed fibres evade stress by buckling, leading to 'slack' (large deformation at low forces) in the network on force reversal (Supplementary Movie 2).

Incomplete recovery due to plastic deformations

To distinguish between a viscous versus plastic origin of the incomplete shape recovery, we use a multidirectional high-force magnetic tweezer device that enables us to investigate the reversibility of the cell deformation, and thus the underlying dissipative mechanism. In the case of a viscous process, we expect that the magnitude of the incomplete recovery decreases when we apply a second force of the same magnitude and duration, but in the opposite direction. In the case of a plastic process, we expect that the magnitude of the incomplete recovery will not decrease, but instead will grow with each reversal of the force direction. Our data show an increase in the residual deformation with each alternating force cycle (Fig. 1c,d), indicating that a plastic and not a viscous process is responsible for the incomplete recovery. This increase in the residual deformation amplitude is consistent with a weak power law versus force cycle number, which is roughly equivalent to time, as all cycles have similar durations.

Timescale invariance of plastic and viscoelastic responses

To describe the cell deformation both during and after force application, we separate the viscoelastic part of the creep response that obeys Boltzmann superposition, $d_{ve}(t)$, from the plastic response, $d_{pl}(t)$, that does not obey Boltzmann superposition. The total cell deformation is the sum of both components $d(t) = d_{ve}(t) + d_{pl}(t)$, as illustrated in Fig. 2b. If the total creep response $d(t)$ is a power law with exponent β , it follows that both $d_{ve}(t)$ and $d_{pl}(t)$ are also power laws with the same exponent. Hence, the creep response during force application is

$$d(t) = (c_{ve} + c_{pl})\Delta F(t/t_0)^\beta \quad (1)$$

with c_{ve} and c_{pl} being the viscoelastic and plastic cell compliance, respectively, after a force duration of $t_0 = 1$ s.

The cell response after the force has been removed at $t = t_1$ is then

$$d(t) = c_{ve}\Delta F[(t/t_0)^\beta - ((t - t_1)/t_0)^\beta] + c_{pl}\Delta F(t_1/t_0)^\beta \quad (2)$$

The first part of the right-hand side describes the viscoelastic response according to the Boltzmann superposition principle, and the second part describes the plastic deformation that is 'frozen' when the force is removed at $t = t_1$ (Fig. 2b). With only three parameters, c_{ve} , c_{pl} and β , it is possible to accurately fit the deformation response both during and after force application. A superposition of elastic and inelastic behaviour during cell deformations has been previously suggested²³, but the inelastic element in their description recovers its original shape after force removal, giving rise to a fully reversible viscoelastic cell response, which is in conflict with our data.

To test the validity of equations (1) and (2), we apply multiple (up to six) force steps of 3 s duration with a 10 s pause. We are able to describe the deformation of individual cells during both the first and subsequent force steps, as well as during force recovery with the same three parameters, c_{ve} , c_{pl} and β (Fig. 2d). The quality of the fit to the data from individual cells is in most cases excellent (Supplementary Fig. 1), with $r^2 = 0.96$ (mean for $n = 60$ cells). A similarly excellent fit is obtained also for the average response of many cells (Fig. 2e), with $r^2 = 0.98$ ($n = 60$ cells).

To verify that the viscoelastic and the plastic component follow the same power law in time, that is, with the same exponent, we alter the total duration of force application between 100 ms and 10 s, followed by a 10 s relaxation. With the same three parameters, we can account for the cell deformation during and after force application in all cases (Fig. 3a), which confirms that the viscoelastic and the plastic part of the creep response follow the same power law and are both timescale invariant. Among a population of cells, the

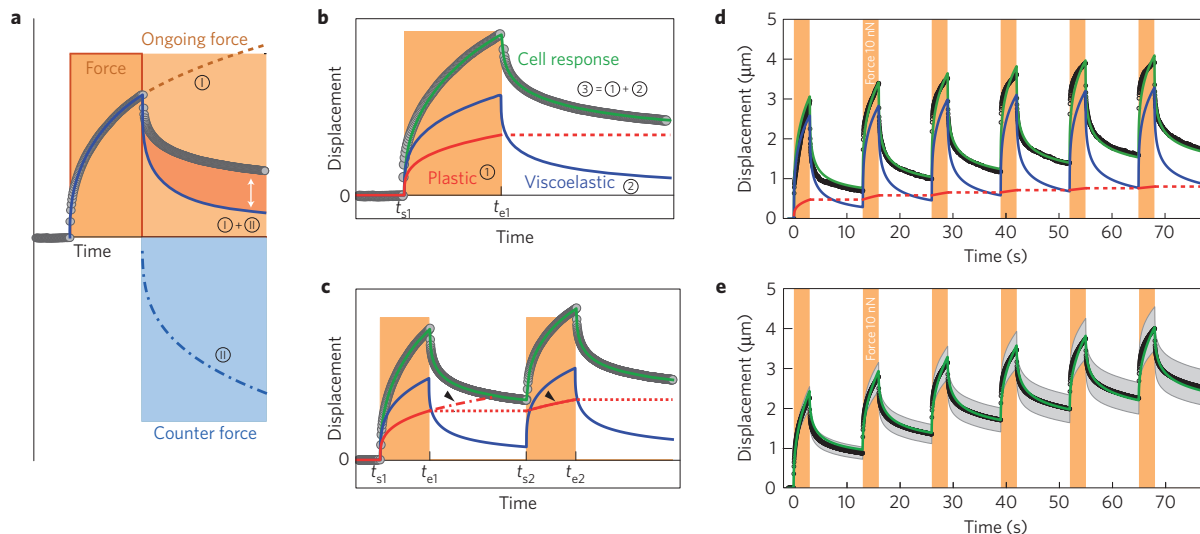


Figure 2 | Superposition of viscoelastic and plastic power-law responses. **a**, During force application (dark orange area), bead displacements (grey circles, measured from a representative cell) can be fitted with a power law (blue line, (I)). This power law, however, fails to predict the bead recovery after force application (blue line, (I) + (II)). According to the Boltzmann superposition principle, the bead displacement after force cessation is the sum of the ongoing power-law creep response to a continuing force (dashed orange line (I)) and the same power-law creep response to a force of the same magnitude but in the opposite direction (dash-dotted blue line (II)). **b**, The total bead displacement (green) can be decomposed into a viscoelastic component that conforms to Boltzmann superposition (blue), and a plastic component (red) that remains constant during the relaxation process (dashed red line). Both components follow a power law with the same exponent. **c**, The cell response to a second force step (grey circles) can be predicted from the sum (green) of the viscoelastic (blue) and the plastic (red) deformation. The plastic deformation resumes the power-law creep process that has paused during the relaxation period (dashed red line). **d**, Cell deformations during multiple force cycles can be described with only three parameters, corresponding to the compliance c_{ve} of the viscoelastic component (blue), the compliance c_{pl} of the plastic component (red), and the power-law exponent β . The quality of the fit (green) to the data of a single cell (black) is excellent, with $r^2 = 0.97$. **e**, The cell deformation of $n = 60$ cells (mean (black circles) \pm s.e.m. (grey area)) in response to multiple force steps can be described by the same fit function (green, $r^2 = 0.98$).

viscoelastic compliance c_{ve} shows a log-normal distribution (Fig. 3c), while the power-law exponent β shows a normal distribution (Fig. 3d), consistent with previous reports^{20,24}. Interestingly, also the plastic compliance c_{pl} shows a log-normal distribution (Fig. 3e), similar to that of c_{ve} , suggesting that c_{pl} and c_{ve} are coupled.

Plastic deformation scales with the total deformation

When we increase the force magnitude of a 3 s force step from 1 to 20 nN, we find that both the viscoelastic and the plastic deformations increase approximately linearly with force (Fig. 3b). Moreover, under all experimental conditions, the ratio c_{pl}/c_{ve} remains approximately constant. The plastic cell deformations are therefore a constant fraction of the total deformation amplitude, regardless of whether the total deformation amplitude has increased because of a higher force, because of a longer duration of force application, or because the force has been applied repeatedly. Together, these findings indicate that plastic responses are tightly linked to the viscoelastic responses, and that both originate from the same structural elements.

To test if the cytoskeleton is the dominant structural element of both elastic and plastic responses, we measure the displacement field of fluorescently labelled actin in fibroblasts during and after force application through integrin-bound magnetic beads. Actin network displacements during force applications are largest near the bead, but remain substantial at considerable distances away from the bead (Fig. 4a), in particular along the orientation of stress fibres. We verify this by tracking the force-induced movements of 1 μ m marker beads surrounding a magnetic bead (Supplementary Figs 2–4). Such anisotropic behaviour has been previously reported and is attributable to actin stress fibres that carry the dominant part of intracellular tensile stress²⁵. Moreover, when stress fibres and forces are aligned (Fig. 4a), non-affine behaviour becomes apparent: displacements of the actin fibres occur predominantly

in the tensed regions, but are smaller in the compressed regions. This is because stress fibres, as other semiflexible filamentous fibres, can carry substantial tensile stresses but buckle when compressed²⁶. When the force is removed, the residual deformations in the actin cytoskeleton are a nearly constant fraction of the maximum local deformations during force application (Fig. 4b). This is consistent with the interpretation that the compressed regions do not generate sufficient restoring forces, because they have evaded elastic stresses through buckling, while the tensed regions have undergone a plastic deformation.

The magnitude of the creep response, however, depends on the cytoskeletal structures to which the beads are connected. For example, data from cell-internalized magnetic beads after incubation for 24 h show that both the viscoelastic and plastic compliance are increased (Supplementary Fig. 5). Both also increase in concert with an increasing compliance of the cell culture substrate (Supplementary Fig. 6), which is known to reduce stress fibre formation and to increase cytoskeletal turnover dynamics²⁷. Together, these data support the notion that the plastic and viscoelastic behaviour in cells is tightly coupled and originates from cytoskeletal structures.

Influence of stress fibre anisotropy and dynamics

To further characterize the contribution of actin stress fibres to cell plasticity, we perform experiments on elongated cells where forces are applied either along or perpendicular to the direction of stress fibre orientation (Fig. 5a,b). The mechanical strain of the tensed stress fibres can be approximated as the bead deformation amplitude divided by the stress fibre length times the cosine of the angle between force and stress fibre orientation. It follows that fibres aligned in the force direction are strained considerably more than fibres aligned perpendicular to the force direction. Therefore, fibres aligned in the force direction are expected to display a larger residual deformation after force removal. Our data confirm this expectation

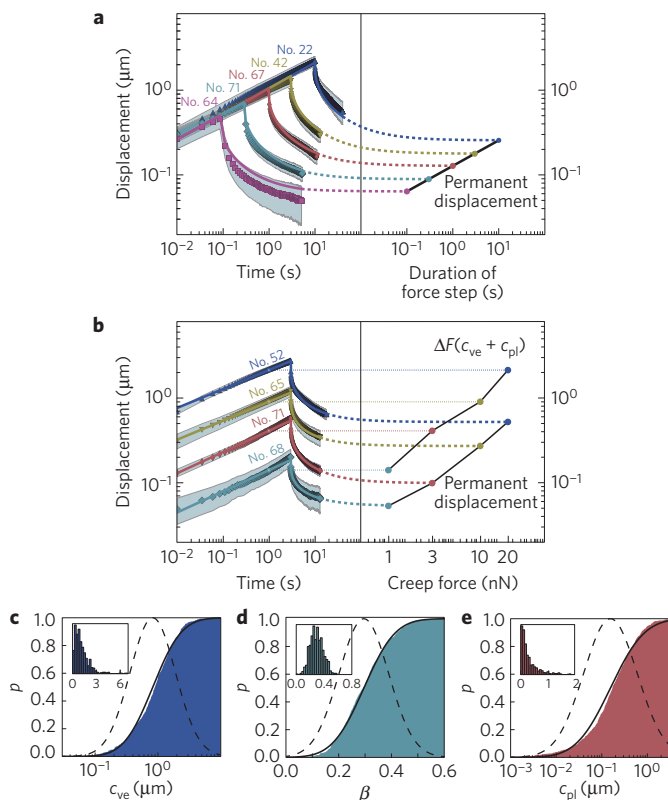


Figure 3 | Timescale invariance and force dependency. **a, b**, Bead displacement versus time (mean (black symbols) \pm s.e.m. (grey area), number of cells as indicated above the curves; logarithmic scale) in response to step forces with different durations and magnitudes. **a**, Cell response to a force step of 10 nN with durations t_1 between 0.1 s and 10 s. With the same three parameters for all measurements, equation (1) describes the cell response over two decades in time (solid lines, r^2 between 0.94 and 0.99). The extrapolation of equation (2) to $t \rightarrow \infty$ (dashed lines) corresponds to the incomplete recovery (permanent deformation) due to plasticity ($c_{pl}\Delta F(t_1/t_0)^\beta$). Hence, the permanent deformation increases as a power law with the duration of force application (black line). **b**, Cell response to a force step with a duration $t_1 = 3$ s and magnitudes between 1 and 20 nN (mean (black symbols) \pm s.e.m. (grey area), number of cells as indicated above the curves; logarithmic scale). For each force, the response was fitted with equation (2) and extrapolated to $t \rightarrow \infty$ (dashed lines) to visualize the permanent deformation (lower black line). Bead displacement after a force duration of 1 s (thin dashed lines) equals the force magnitude times the total compliance $\Delta F(c_{ve} + c_{pl})$ (upper black line). Both lines increase with the same slope, indicating that plastic deformations are a constant fraction of the total deformations. **c–e**, Cumulative distribution and probability density (inset) of the parameters c_{ve} (**c**), β (**d**) and c_{pl} (**e**) fitted to the responses of individual cells shown in **a, b**. Distributions of c_{ve} , c_{pl} (shaded area, not normalized by force) can be described by a log-normal distribution (note the logarithmic scaling of the x-axis), and β by a normal distribution (black lines). The corresponding probability density functions are normalized to unity and are shown by the dashed lines.

(Fig. 5c,d). In agreement with previous reports, this mechanical alignment is accompanied by a transition of the cytoplasm to be more fluid-like along the flow direction and more solid-like along the perpendicular direction²⁸.

If the plastic deformations originate from force- and deformation-induced structural rearrangements such as slippage and breakage of inter- and intrafilament crosslinks or integrin–cytoskeleton links, as suggested in ref. 22, we expect that

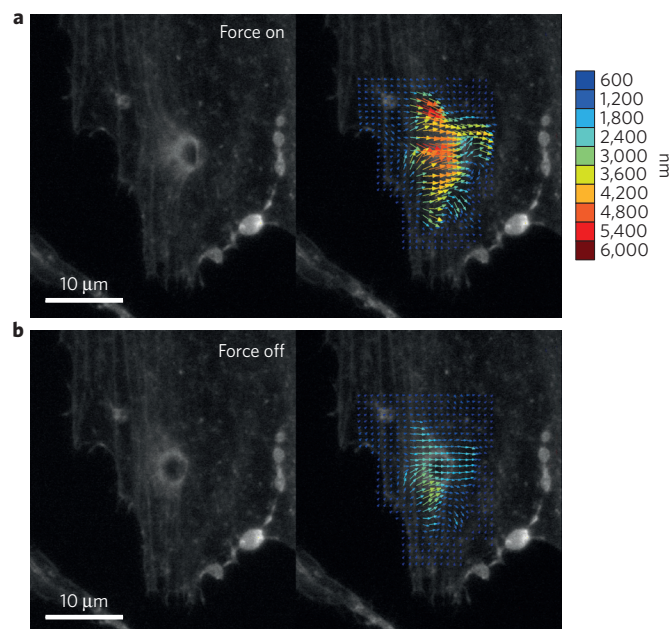


Figure 4 | Deformation map of the actin network. **a, b**, Fluorescence image of the actin cytoskeleton during force application with a magnetic bead (**a**), and 35 s after the force has been removed (**b**). Deformation amplitude and deformation direction relative to the undeformed cytoskeleton are indicated by the length and colour of arrows (see Supplementary Movie 3).

cell plasticity and energy dissipation during force application are closely related. The dissipative properties of cells are characterized by the power-law exponent β of the creep response, where values of 0 describe elastic solid-like behaviour, and values of 1 describe viscous fluid-like behaviour. Moreover, the power-law exponent in cells is related to the stability of cytoskeletal bonds⁵ and can be altered by pharmacological interventions. We therefore change the stability of cytoskeletal bonds by adding increasing concentrations of the crosslinker paraformaldehyde to the cells, and measure the power-law exponent β and the relative plasticity $c_{pl}/(c_{ve} + c_{pl})$ during and after a step force (Fig. 5e). We find that with increasing concentrations of the crosslinker, both the power-law exponent β and the relative plasticity decrease, thus confirming that plastic deformations originate from bond slippage or breakage. We find a similar scaling behaviour between the power-law exponent β and the relative plasticity also for different cell types and for cells cultured on differently stiff substrates (Supplementary Fig. 8), although the absolute values for the viscoelastic and plastic compliance vary over a large range (Supplementary Fig. 9).

In summary, our data reveal pronounced plastic rheological behaviour in living cells. The recovery of the cell shape after a temporal force application is incomplete, with a residual deformation that is proportional to the total deformation amplitude. This plastic deformation displays the same timescale-invariant dynamics as the viscoelastic deformations, and thus cannot be attributed to purely viscous responses of the cell. Rather, our data indicate that plastic cell responses originate from bond ruptures within the cytoskeleton. Restoring cell shape after mechanical loading is of fundamental importance for maintaining cell integrity. At the same time, an incomplete shape recovery is an adaptive process, as it reduces cell mechanical stresses during subsequent deformations and therefore protects the cell against mechanical damage.

Methods

Methods and any associated references are available in the [online version of the paper](#).

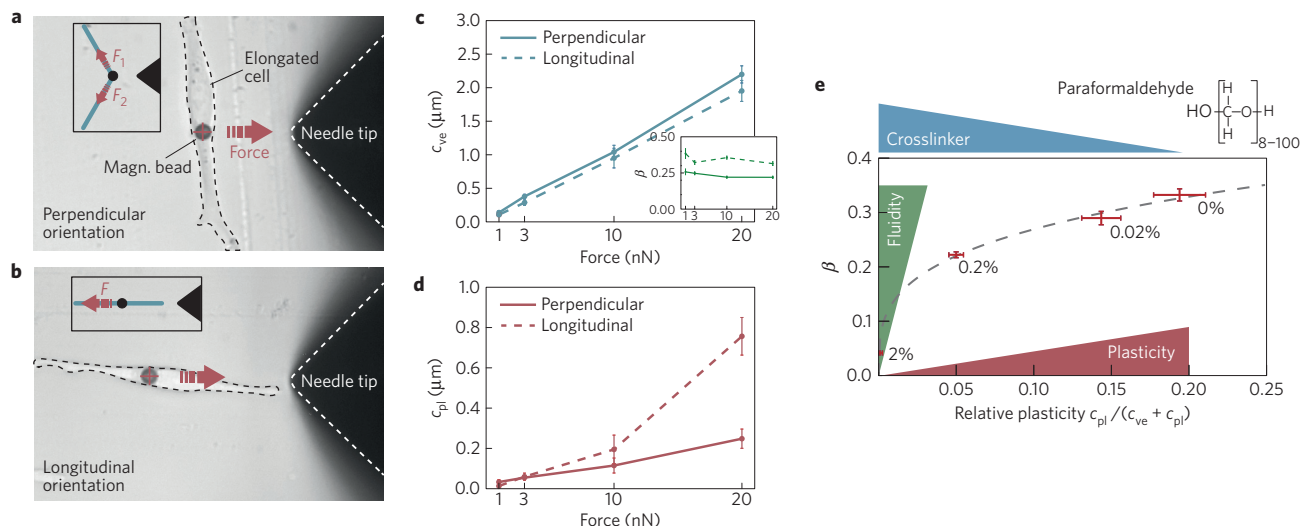


Figure 5 | Dependence of plasticity on actin fibre orientation and stability. **a, b**, Creep experiment performed perpendicular (**a**) and longitudinal (**b**) to the stress fibre orientation of elongated cells. **c**, Viscoelastic compliance (not normalized by force) and power-law exponent β (inset) for perpendicular and longitudinal force direction (mean \pm s.e.m., $n = 41, 42, 28$ (perpendicular), 68, 71, 65, 52 (longitudinal) for the 1, 3, 10, 20 nN force protocol, respectively). **d**, Plastic compliance for perpendicular and longitudinal force direction (mean \pm s.e.m. of the same cells). Corresponding mean displacement curves are shown in Supplementary Fig. 7. **e**, Relative plasticity and power-law exponent β for cells treated with different concentrations of the crosslinker paraformaldehyde. Both plasticity and power-law exponent decrease with increasing crosslinker concentration.

Received 11 November 2014; accepted 1 June 2016;
published online 4 July 2016

References

- Fabry, B. *et al.* Scaling the microrheology of living cells. *Phys. Rev. Lett.* **87**, 148102 (2001).
- Wolf, K. *et al.* Physical limits of cell migration: control by ECM space and nuclear deformation and tuning by proteolysis and traction force. *J. Cell Biol.* **201**, 1069–1084 (2013).
- Wang, N. *et al.* Cell prestress. I. Stiffness and prestress are closely associated in adherent contractile cells. *Am. J. Physiol. Cell Physiol.* **282**, C606–C616 (2002).
- Kollmannsberger, P. & Fabry, B. Linear and nonlinear rheology of living cells. *Annu. Rev. Mater. Res.* **41**, 75–97 (2011).
- Bursac, P. *et al.* Cytoskeletal remodelling and slow dynamics in the living cell. *Nature Mater.* **4**, 557–561 (2005).
- Trepat, X., Lenormand, G. & Fredberg, J. J. Universality in cell mechanics. *Soft Matter* **4**, 1750–1759 (2008).
- Bouchaud, J. Weak ergodicity breaking and aging in disordered systems. *J. Phys. I* **2**, 1705–1713 (1992).
- Sollich, P., Lequeux, F., Hébraud, P. & Cates, M. E. Rheology of soft glassy materials. *Phys. Rev. Lett.* **78**, 2020–2023 (1997).
- Mak, M. & Erickson, D. A serial micropipette microfluidic device with applications to cancer cell repeated deformation studies. *Integr. Biol.* **5**, 1374–1384 (2013).
- Bausch, A. R., Ziemann, F., Boulbitch, A. A., Jacobson, K. & Sackmann, E. Local measurements of viscoelastic parameters of adherent cell surfaces by magnetic bead microrheometry. *Biophys. J.* **75**, 2038–2049 (1998).
- Bausch, A. R., Moller, W. & Sackmann, E. Measurement of local viscoelasticity and forces in living cells by magnetic tweezers. *Biophys. J.* **76**, 573–579 (1999).
- Butler, J. P. & Kelly, S. M. A model for cytoplasmic rheology consistent with magnetic twisting cytometry. *Biorheology* **35**, 193–209 (1998).
- Tschumperlin, D. J. & Margulies, S. S. Equibiaxial deformation-induced injury of alveolar epithelial cells *in vitro*. *Am. J. Physiol. Lung Cell Mol. Physiol.* **275**, L1173–L1183 (1998).
- Fredberg, J. J. Airway obstruction in asthma: does the response to a deep inspiration matter? *Respir. Res.* **2**, 273–275 (2001).
- Summers, C. *et al.* Pulmonary retention of primed neutrophils: a novel protective host response, which is impaired in the acute respiratory distress syndrome. *Thorax* **69**, 623–629 (2014).
- Trepat, X. *et al.* Universal physical responses to stretch in the living cell. *Nature* **447**, 592–595 (2007).
- Smith, B. A., Tolloczko, B., Martin, J. G. & Grutter, P. Probing the viscoelastic behavior of cultured airway smooth muscle cells with atomic force microscopy: stiffening induced by contractile agonist. *Biophys. J.* **88**, 2994–3007 (2005).
- Balland, M. *et al.* Power laws in microrheology experiments on living cells: comparative analysis and modeling. *Phys. Rev. E* **74**, 021911 (2006).
- Maloney, J. M. *et al.* Mesenchymal stem cell mechanics from the attached to the suspended state. *Biophys. J.* **99**, 2479–2487 (2010).
- Fabry, B. *et al.* Time course and heterogeneity of contractile responses in cultured human airway smooth muscle cells. *J. Appl. Physiol.* **91**, 986–994 (2001).
- Hildebrandt, J. Comparison of mathematical models for cat lung and viscoelastic balloon derived by Laplace transform methods from pressure-volume data. *Bull. Math. Biophys.* **31**, 651–667 (1969).
- Bausch, A. R., Hellerer, U., Essler, M., Aepfelbacher, M. & Sackmann, E. Rapid stiffening of integrin receptor-actin linkages in endothelial cells stimulated with thrombin: a magnetic bead microrheology study. *Biophys. J.* **80**, 2649–2657 (2001).
- Fernandez, P. & Ott, A. Single cell mechanics: stress stiffening and kinematic hardening. *Phys. Rev. Lett.* **100**, 238102 (2008).
- Desprat, N., Richert, A., Simeon, J. & Asnacios, A. Creep function of a single living cell. *Biophys. J.* **88**, 2224–2233 (2005).
- Hu, S. *et al.* Intracellular stress tomography reveals stress focusing and structural anisotropy in cytoskeleton of living cells. *Am. J. Physiol. Cell Physiol.* **285**, C1082–C1090 (2003).
- Munster, S. *et al.* Strain history dependence of the nonlinear stress response of fibrin and collagen networks. *Proc. Natl Acad. Sci. USA* **110**, 12197–12202 (2013).
- Pelham, R. J. Jr & Wang, Y. Cell locomotion and focal adhesions are regulated by substrate flexibility. *Proc. Natl Acad. Sci. USA* **94**, 13661–13665 (1997).
- del Alamo, J. C., Norwich, G. N., Li, Y. S., Lasheras, J. C. & Chien, S. Anisotropic rheology and directional mechanotransduction in vascular endothelial cells. *Proc. Natl Acad. Sci. USA* **105**, 15411–15416 (2008).

Acknowledgements

This work was funded by the Deutsche Forschungsgemeinschaft (DFG) and the European Research Council Starting Grant MINATRAN 211166. We thank A. Mainka for help with cell culture and K. Kroy and M. Gralka for valuable discussions.

Author contributions

N.B., M.K., M.S. and A.L. performed experiments, N.B. and W.S. designed the rotation stage, N.B., K.E.A. and B.F. developed the model, N.B., R.G. and B.F. analysed the data, and N.B., R.G., K.E.A. and B.F. wrote the manuscript.

Additional information

Supplementary information is available in the online version of the paper. Reprints and permissions information is available online at www.nature.com/reprints. Correspondence and requests for materials should be addressed to N.B.

Competing financial interests

The authors declare no competing financial interests.

Methods

Magnetic tweezer. To apply high forces to magnetic beads bound to cells, a magnetic tweezer is used^{4,10}. Briefly, an electromagnet with a sharp-tipped μ -metal core generates a strong magnetic field gradient, and thus a lateral force on the beads, pointing towards the tip. Forces in our set-up are strictly horizontally aligned by lowering the needle tip with a motorized micromanipulator to the height of the bead a few micrometres above the culture plate. We have verified that all force vectors point to the tip of the needle within a cone with an opening angle of 135° (ref. 4). The force is calibrated from the velocity of beads in liquids of known viscosity measured as a function of the tip–bead distance and the applied current. 1 mg of carboxylated super-paramagnetic beads (Microparticles) with $5 \pm 0.21 \mu\text{m}$ diameter are coated with 50 mg ml^{-1} human fibronectin (Roche) in 1 ml of carbonate buffer (pH 9.4) overnight at 4°C . After coating, the beads are washed and stored in PBS. 10,000 cells are plated in 35 mm dishes for 24 h, and fibronectin-coated beads are then added to the cells and incubated for 30 min at 37°C and 5% CO_2 . Before measurements, the dishes are gently washed with fresh medium to remove unbound beads. In addition, beads that detached from the cell surface during force application were not included in the analysis.

With the magnetic tweezer, different force steps of different duration and amplitude can be applied to the beads. Bright-field images of the cell, the bead, and the needle tip are taken with a charge-coupled device (CCD) camera (ORCA ER Hamamatsu) at a rate of 40 frames per second at $\times 40$ magnification. Bead positions are tracked in real time using an intensity-weighted centre-of-mass algorithm.

Rotational stage. To apply multidirectional forces to cells, the cell well is placed on a rotational stage driven by a stepper motor. The rotational stage is placed on a motorized x – y microscope stage (Märzhäuser) to automatically keep the distance between the magnetic bead and the tweezer tip constant after rotation (see Supplementary Movie 1).

Cells. For all experiments except where specified otherwise, we use NIH3T3 mouse embryonic fibroblasts which are maintained in DMEM (1 g l^{-1} D-glucose) with 10% fetal calf serum (FCS, Greiner), 1% penicillin–streptomycin (Greiner) at 37°C , 5% CO_2 and 95% humidity. For measuring the cytoskeletal deformation field, mouse embryonic fibroblasts (MEF) stably transfected with an F-actin green fluorescent protein (GFP)-tagged construct are used. Cells are maintained in high-glucose Dulbecco's modified Eagle's medium (DMEM 4.5 g glucose, Greiner) with 10% FCS and 1% penicillin–streptomycin in 75 cm^2 cell culture flasks. Due to the puromycin resistance in the GFP–actin construct, $0.1 \mu\text{g}$ puromycin (Sigma) is added to 500 ml DMEM to select transfected cells.

GFP–actin displacements. Actin displacements in the cell during and after force application are measured by image particle velocimetry: 32×32 pixel segments from the reference image (taken before force application) are cross-correlated with corresponding 64×64 pixel segments of the target image (taken during or after force application). The position of the highest cross-correlation is taken as the displacement of the image segment.

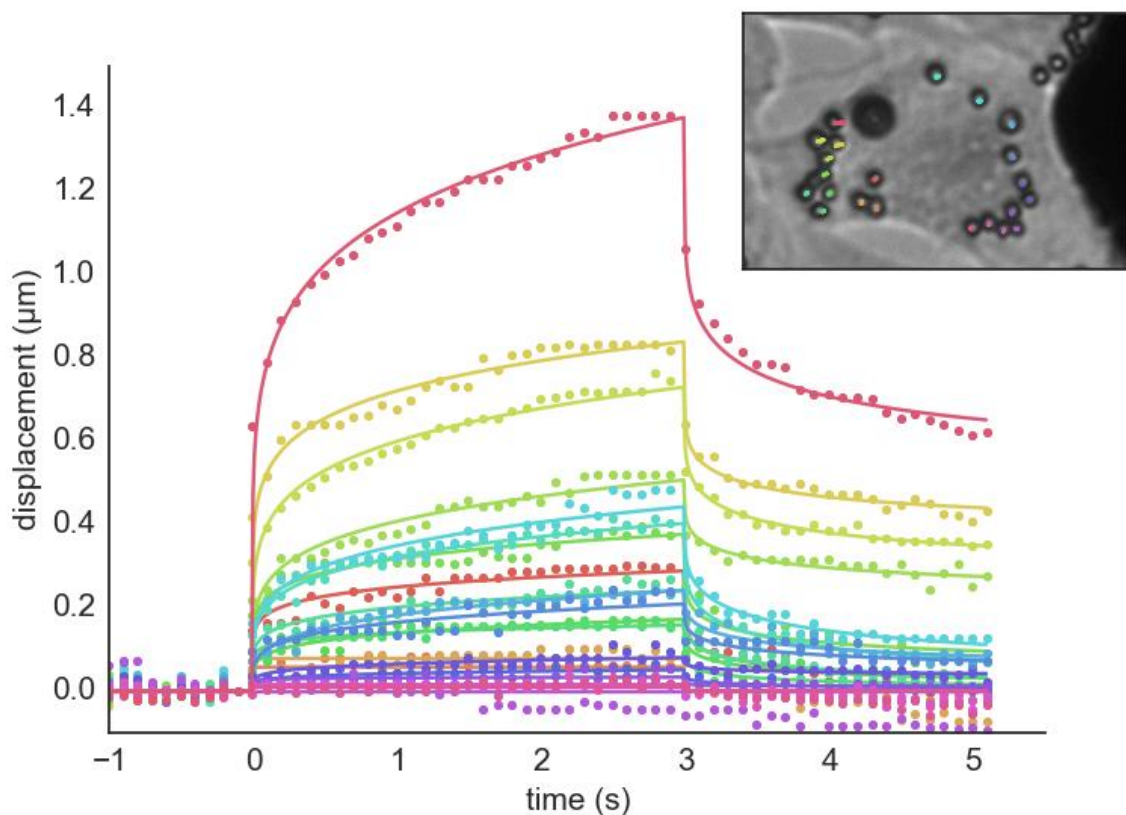
Mechanical plasticity of cells

Navid Bonakdar^{1*}, Richard Gerum^{1*}, Michael Kuhn¹, Marina Spörrer¹, Anna Lippert¹,
Werner Schneider¹, Katerina E. Aifantis², Ben Fabry¹

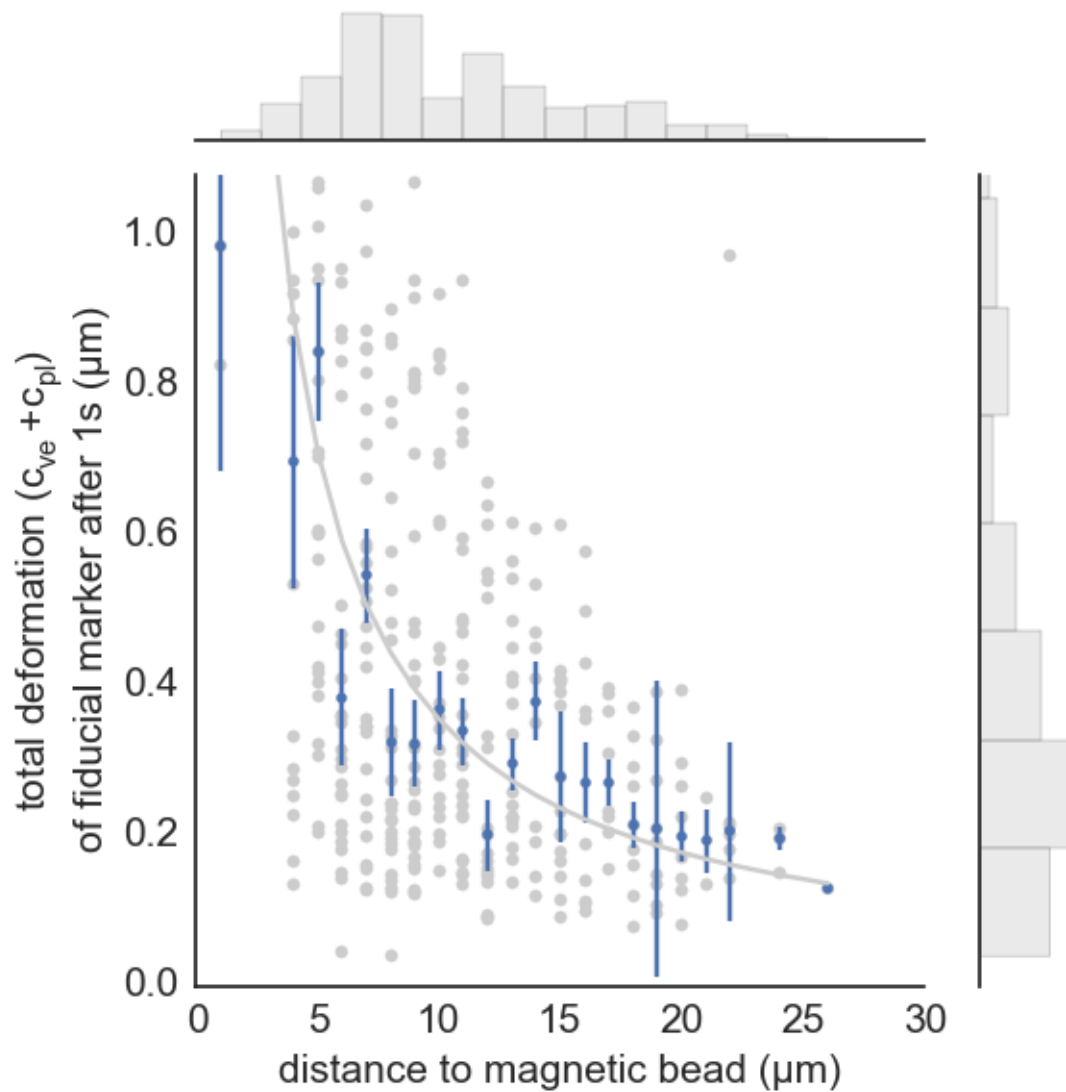
¹Department of Physics, University of Erlangen-Nuremberg, Erlangen, Germany

²Department of Civil Engineering and Engineering Mechanics, University of Arizona, Tucson, AR, USA

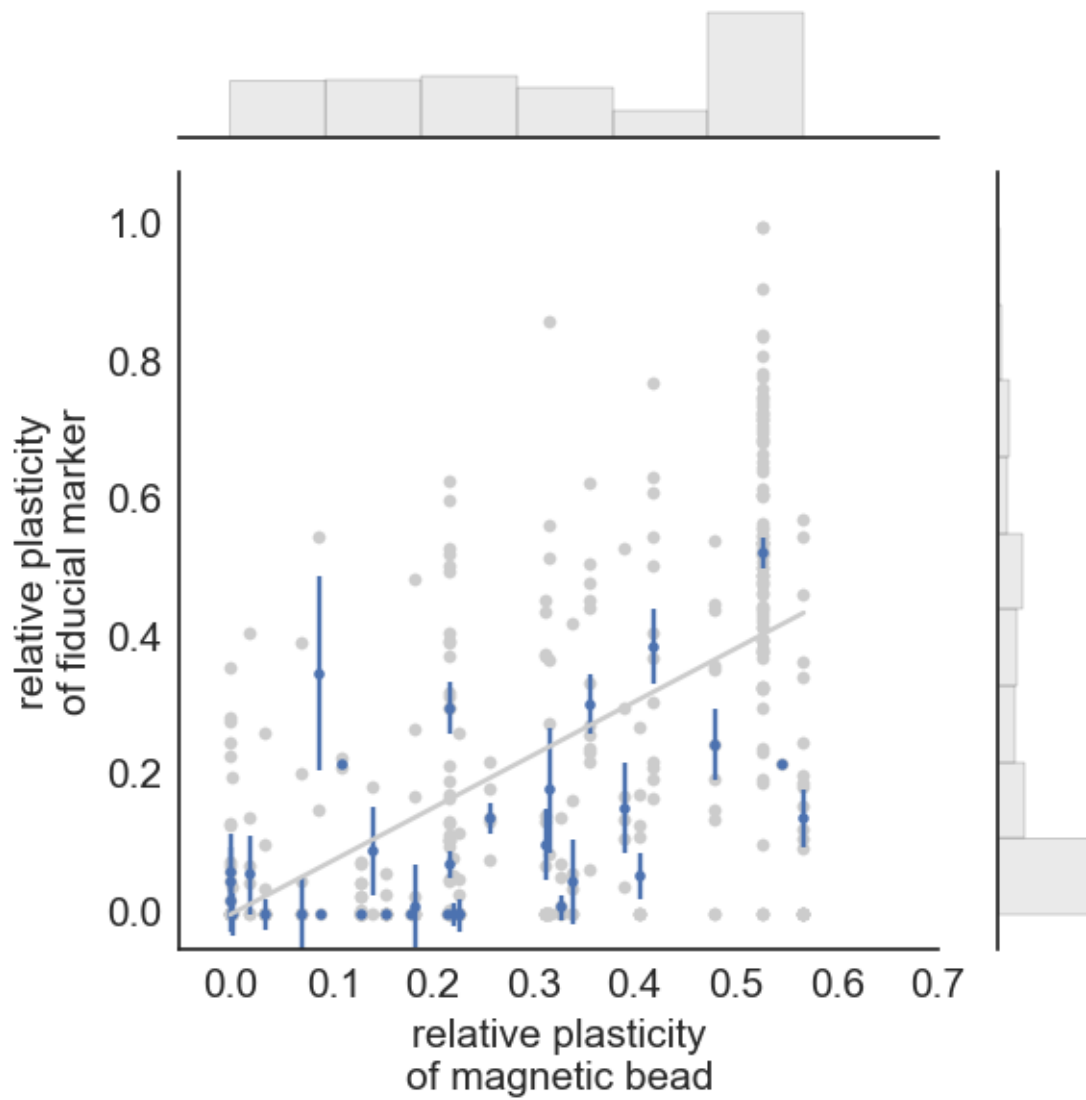
*These authors contributed equally to this work.



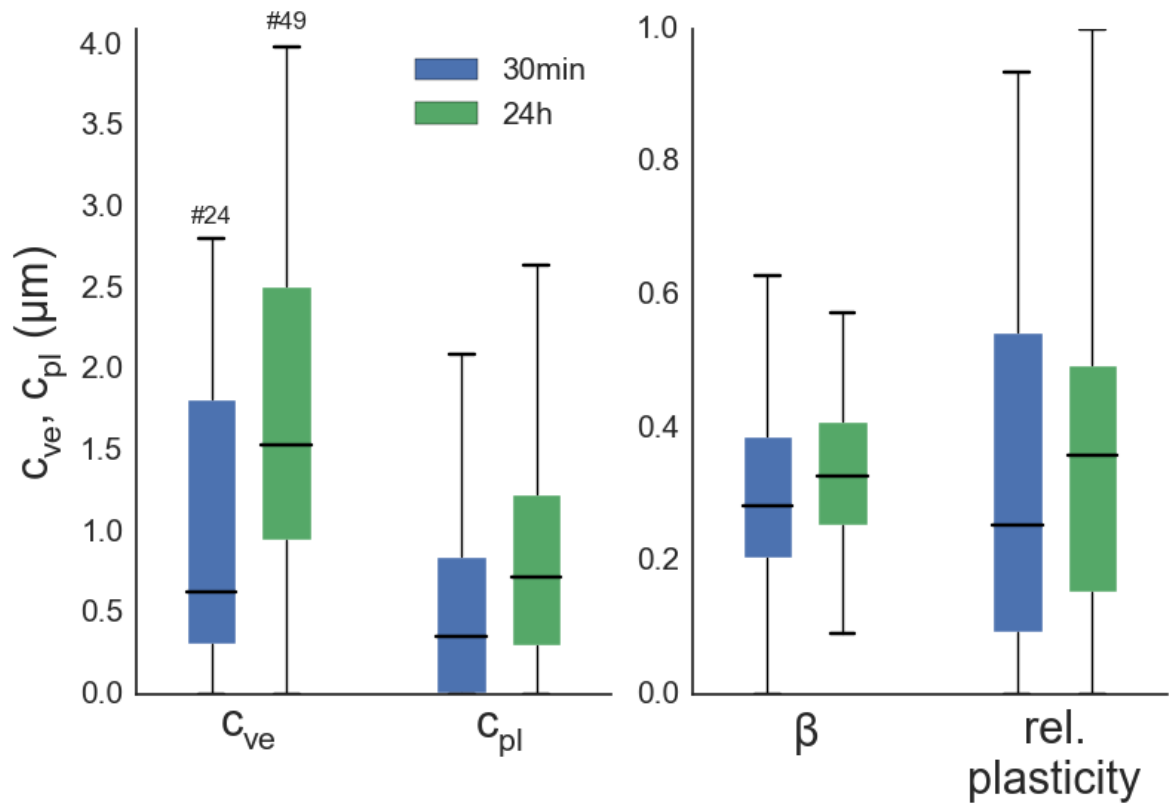
Supplementary Figure 2 | Displacement curves of fiducial marker beads. Magnetic tweezer measurements are performed with MEF cells additionally labelled for 30 min with small ($1\ \mu\text{m}$) non-magnetic fibronectin-coated beads ^{1,2} (see inset). Movements of fiducial marker beads (Supplementary Movie 4) are tracked using the ClickPoints software by marking the starting positions manually and updating the position using a sparse iterative Lucas-Kanade optical flow algorithm ³. Marker displacements in x-direction (towards the magnetic tweezer needle) (circles) are fitted using Equ. (1) and (2) (solid lines). The colors in the plot from a representative cell correspond to colors shown in the inset.



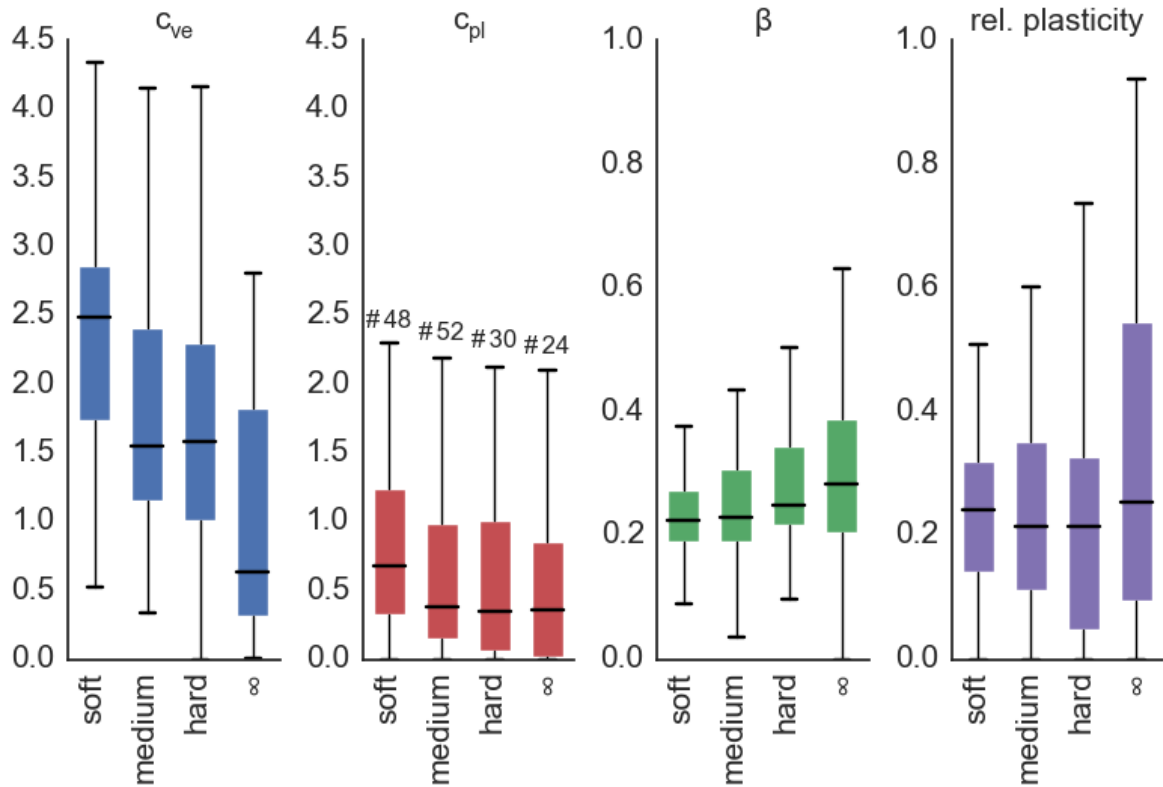
Supplementary Figure 3 | Displacements of fiducial markers decrease with distance to the magnetic bead. Total compliance ($c_{ve} + c_{pl}$) of the fiducial marker beads is plotted versus their distance to the magnetic bead (each gray dot corresponds to a marker bead, mean and sd (blue) over bins of 1 μm , data from 34 cells). With increasing distance, the displacements of the fiducial marker beads decrease.



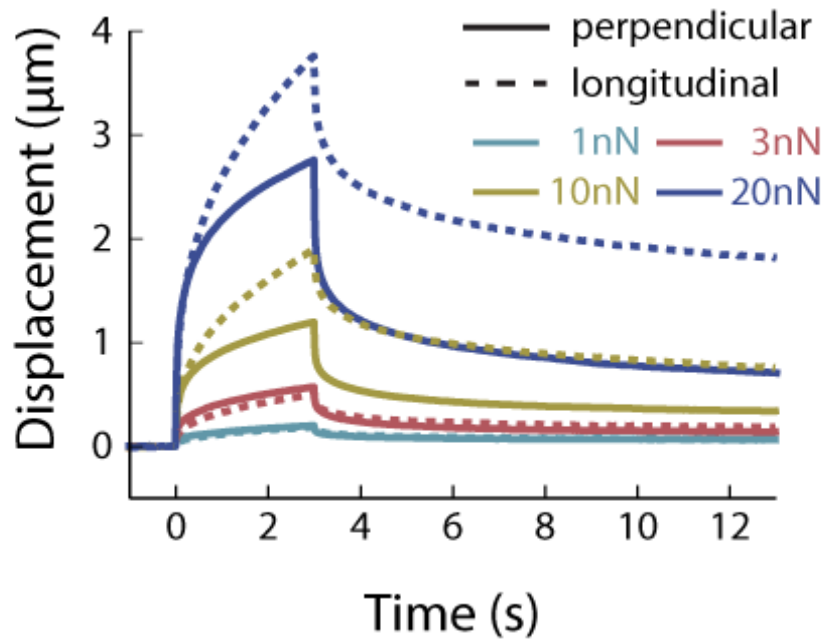
Supplementary Figure 4 | Relative plasticity of fiducial marker correlates with the relative plasticity of the magnetic bead. Relative plasticity of fiducial marker beads plotted versus the relative plasticity of the magnetic bead from the same cell (each gray dot corresponds to a marker bead, mean and sd (blue) of 34 cells).



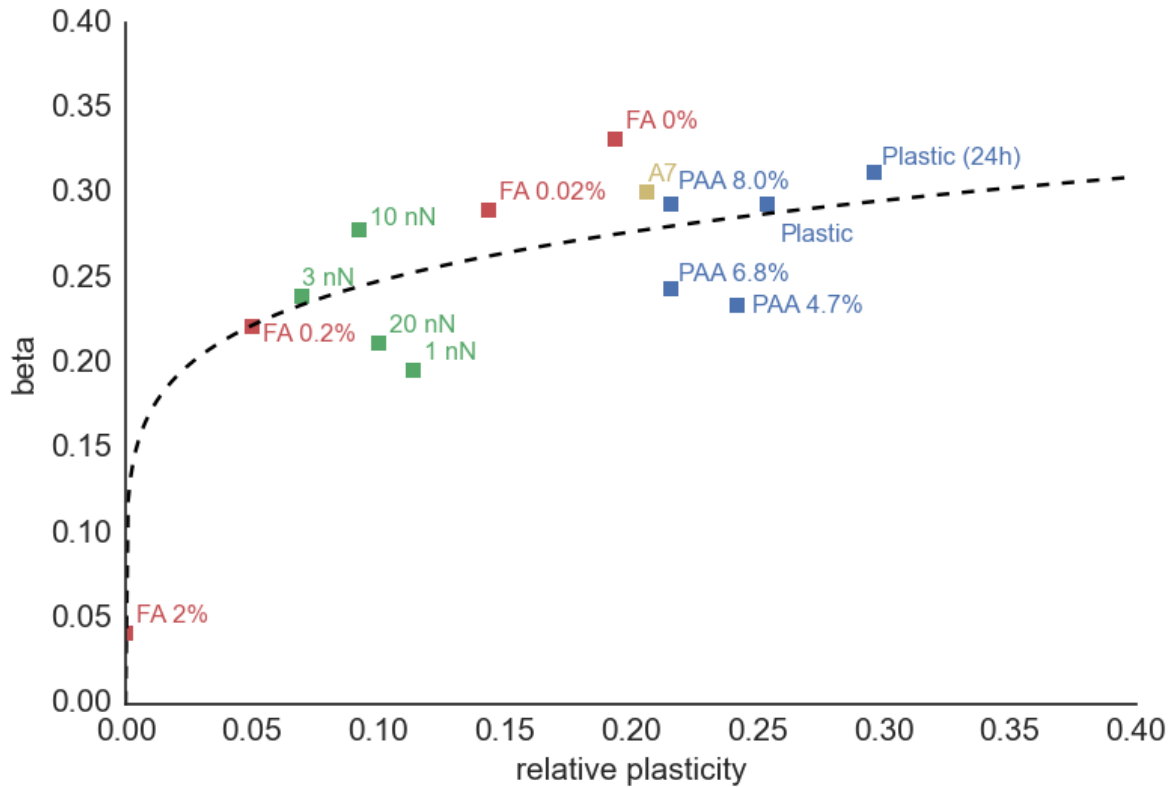
Supplementary Figure 5 | Effect of bead adhesion times. Magnetic tweezer measurements (10 nN force) are performed with different incubation times (30 min or 24 h) after adding magnetic beads to the cells (median (black line), 25-75 percentile (box), 95 percentile (bars), number of cells as indicated above bar). Cells with beads incubated for 24 h show an increased viscoelastic and plastic compliance.



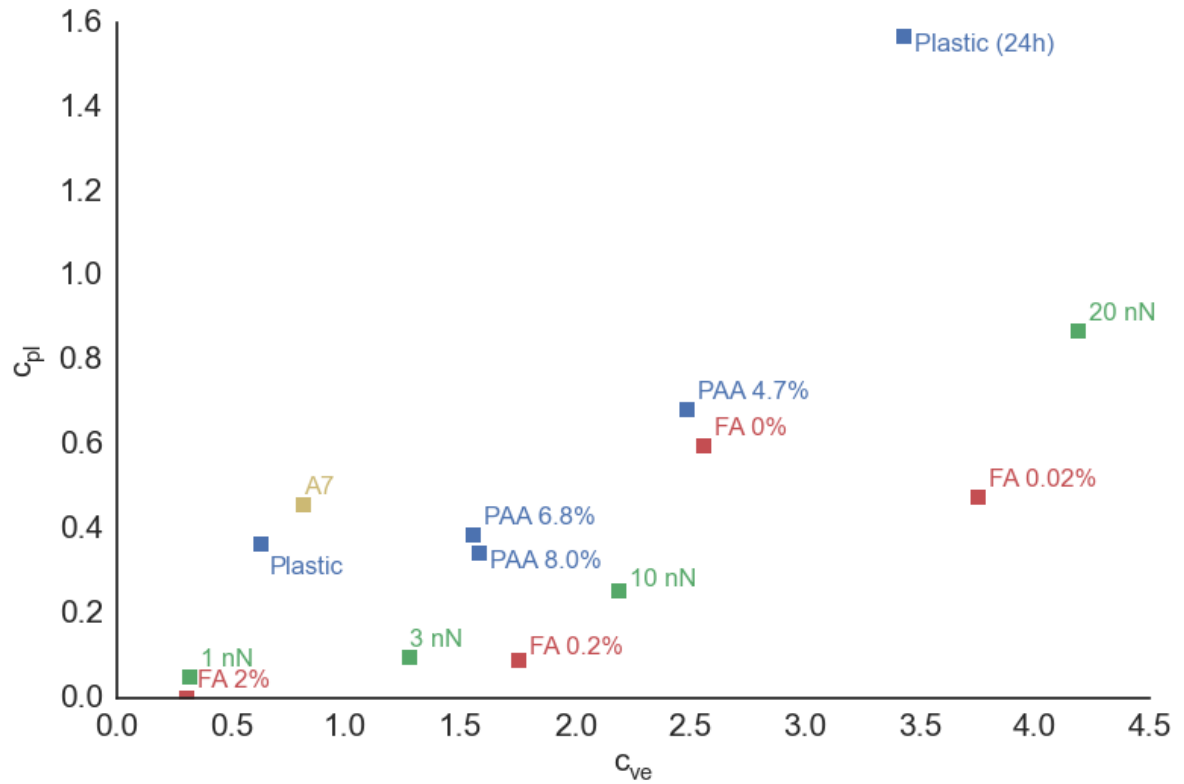
Supplementary Figure 6 | Effect of substrate stiffness on cell properties. Magnetic tweezer measurements are performed with cells seeded on differently stiff substrates: 4.7% PAA 4.6 kPa (soft), 6.8% PAA 22.5 kPa (medium), 8.0% PAA 56.1 kPa (hard) and tissue culture plastic coated with fibronectin (∞) (median (black line), 25-75 percentile (box), 95 percentile (bars), number of cells as indicated above bar). The cells' viscoelastic (c_{ve}) and plastic (c_{pl}) compliance (measured at 10 nN) decreases, and the power-law exponent (β) increases with substrate stiffness. The relative plasticity $c_{pl}/(c_{ve}+c_{pl})$ is insensitive to the substrate stiffness.



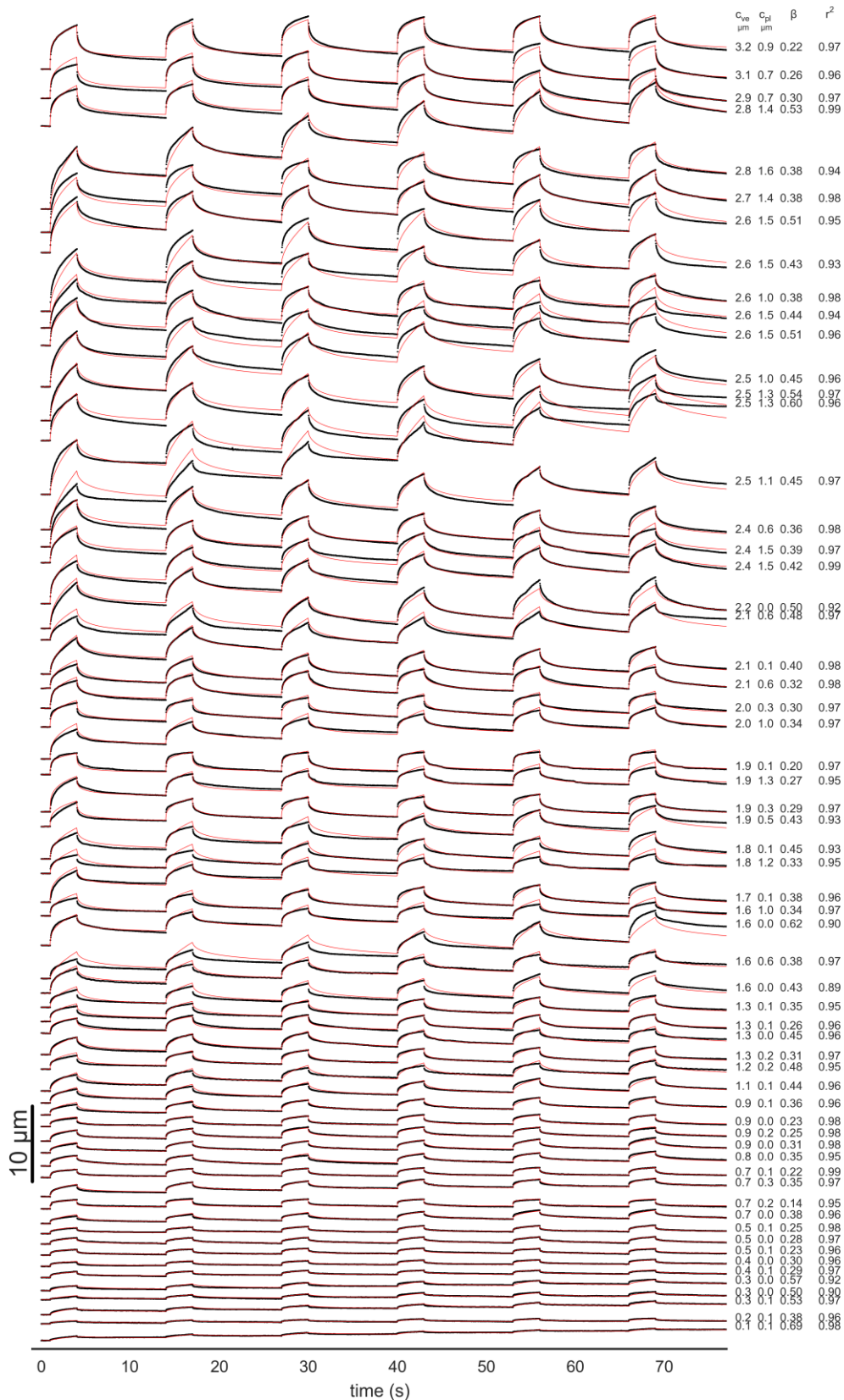
Supplementary Figure 7 | Displacement curves for vertical and perpendicular force applications. Mean displacement for forces of 1 (cyan), 3 (red), 10 (yellow) and 20 (blue) nN for 3 seconds for perpendicular (solid lines) and longitudinal (dashed lines) force application protocol. (cell numbers are 41, 42, 42, 28 (perp.), 68, 71, 65, 52 (long.) cells for 1, 3, 10, 20 nN).



Supplementary Figure 8 | Power-law exponent vs. relative plasticity for different cell lines and conditions: NIH3T3 cells for different forces (green, data from Fig. 3), increasing concentration of paraformaldehyde (red, data from Fig. 5), 24 h overnight incubation time (dark blue, data from Supplement Fig. 5), cells seeded on substrates with different stiffness (light blue, data from Supplementary Fig. 6), and from A7 melanoma cells (kindly provided by T. Stossel) under standard culture conditions (yellow). Cells under all conditions follow a common relationship (dashed line).



Supplementary Figure 9 | Viscoelastic (c_{ve}) vs. plastic (c_{pl}) compliance for different cell lines and conditions: NIH3T3 cells for different forces (green, data from Fig. 3), increasing concentration of paraformaldehyde (red, data from Fig. 5), 24 h incubation time (dark blue, data from Supplementary Fig. 5), cells seeded on substrates with different stiffness (light blue, data from Supplementary Fig. 6), and from A7 melanoma cells under standard culture conditions (yellow).



Supplementary Figure 10 | Response to multiple force applications. Displacements of individual beads (black circles, $n=60$) attached to NIH3T3 cells in response to multiple force pulses of 10 nN with 3 s duration and 10 s pause. Each curve is fitted (red line) with three parameters (c_{ve} , c_{pl} , β , shown on the right, together with the fit quality r^2) using Equ. (1) and (2).

References

- 1 Bausch, A. R., Ziemann, F., Boulbitch, A. A., Jacobson, K. & Sackmann, E. Local measurements of viscoelastic parameters of adherent cell surfaces by magnetic bead microrheometry. *Biophys J* **75**, 2038-2049 (1998).
- 2 Bausch, A. R., Moller, W. & Sackmann, E. Measurement of local viscoelasticity and forces in living cells by magnetic tweezers. *Biophys J* **76**, 573-579, doi:10.1016/S0006-3495(99)77225-5 (1999).
- 3 Lucas, B. D. & Kanade, T. An iterative image registration technique with an application to stereo vision. *Proceedings of Imaging Understanding Workshop*, 121-130 (1981).